Chapter 2
Stability Charts for Fundamental Delay-Differential Equations

Simple scalar equations play an important role in understanding the main features of DDEs and the function of stability charts. Stability charts are diagrams constructed in the plane of two (or more) parameters of the system showing the stable and unstable domains or the numbers of unstable characteristic exponents/multipliers. In this chapter, some basic scalar equations are considered for which the stability charts can be constructed in closed form by a straightforward analysis of the characteristic equation. In Sections 2.1, 2.2, and 2.3, first- and second-order autonomous scalar DDEs are analyzed by the D-subdivision method, while in Section 2.4, a second-order time-periodic scalar DDE, the delayed Mathieu equation, is analyzed by Hill's infinite determinant method.

2.1 First-Order Scalar Equations

In this section, stability properties of linear first-order scalar DDEs with point delays and with distributed delays are analyzed. The corresponding stability charts are constructed by the D-subdivision method and by analysis of the exponent-crossing directions.

2.1.1 The Hayes Equation

Consider the first-order scalar equation with a single point delay in the form

$$\dot{x}(t) = ax(t) + bx(t-\tau)\ . \tag{2.1}$$

This equation is often referred to as one of the simplest basic examples of a delayed system [153, 255, 188, 251]. The stability condition for the parameters a and b was

T. Insperger and G. Stépán, *Semi-Discretization for Time-Delay Systems: Stability and Engineering Applications*, Applied Mathematical Sciences 178,
DOI 10.1007/978-1-4614-0335-7_2, © Springer Science+Business Media, LLC 2011

first presented by Hayes [104] in 1950. In this section, the stability chart with the numbers of unstable characteristic exponents is constructed in an analytic way.

If $b = 0$, then (2.1) reduces to the scalar ODE

$$\dot{x}(t) = ax(t) \tag{2.2}$$

with the characteristic function

$$D(\lambda) = \lambda - a \; . \tag{2.3}$$

In this case, the only characteristic exponent is $\lambda = a$; consequently, the system is asymptotically stable if $a > 0$, and it is unstable if $a < 0$.

The stability properties for the case $b \neq 0$ are more complex due to the infinite-dimensional nature of the delayed system. The corresponding characteristic function reads

$$D(\lambda) = \lambda - a - b\mathrm{e}^{-\lambda\tau} \; . \tag{2.4}$$

According to the D-subdivision method, substitution of $\lambda = \gamma \pm \mathrm{i}\omega$, $\omega \geq 0$, into the characteristic equation $D(\lambda) = 0$ and decomposition into real and imaginary parts yields

$$\mathrm{Re} \; : \quad \gamma - a - b\mathrm{e}^{-\gamma\tau}\cos(\omega\tau) = 0 \; , \tag{2.5}$$

$$\mathrm{Im} \; : \quad \omega + b\mathrm{e}^{-\gamma\tau}\sin(\omega\tau) = 0 \; . \tag{2.6}$$

The case $\gamma = 0$ gives the D-curves as a parametric function of ω in the form

$$\text{if } \omega = 0 \; : \quad b = -a \; , \tag{2.7}$$

$$\text{if } \omega\tau \neq k\pi \; , \; k \in \mathbb{N} : \quad a = \frac{\omega\cos(\omega\tau)}{\sin(\omega\tau)} \; , \quad b = \frac{-\omega}{\sin(\omega\tau)} \; , \tag{2.8}$$

with the corresponding limits for $\omega\tau = k\pi$, $k \in \mathbb{N}$. The D-curve given by (2.7) is associated with a real critical characteristic exponent crossing the imaginary axis at 0. The D-curves given by (2.8) are associated with a complex conjugate pair of characteristic exponents in the form $\lambda = \pm\mathrm{i}\omega$, where ω is the angular frequency of the arising vibrations.

Due to the continuity of the characteristic exponents with respect to changes in the system parameters, these curves divide the parameter plane (a, b) into regions where the numbers of unstable characteristic exponents are constant. As mentioned in Section 1.3, the change of these numbers along the D-curves can be determined by analysis of the exponent-crossing direction, which is the sign of the partial derivative of γ with respect to one of the system parameters.

Taking the partial derivative of (2.5) and (2.6) with respect to b and considering that $\gamma = 0$ along the D-curves gives

$$(1 + b\tau\cos(\omega\tau))\gamma'_b + (b\tau\sin(\omega\tau))\omega'_b = \cos(\omega\tau) \; , \tag{2.9}$$

$$-(b\tau\sin(\omega\tau))\gamma'_b + (1 + b\tau\cos(\omega\tau))\omega'_b = -\sin(\omega\tau) \; , \tag{2.10}$$

where γ'_b and ω'_b are the partial derivatives of γ and ω with respect to b. The solution of (2.9)–(2.10) for γ'_b is

$$\gamma'_b = \frac{\cos(\omega\tau) + b\tau}{(1 + b\tau\cos(\omega\tau))^2 + (b\tau\sin(\omega\tau))^2} \,. \tag{2.11}$$

For the D-curve (2.7), equation (2.11) gives $\gamma'_b = (1 + b\tau)^{-1}$. If $b > -1/\tau$, then γ'_b is positive; consequently, the critical characteristic exponent crosses the imaginary axis from left to right through the origin as b is increased, i.e., a stable characteristic exponent becomes unstable. If $b < -1/\tau$, then the critical characteristic exponent crosses the imaginary axis in the opposite direction, i.e., an unstable exponent becomes stable for increasing b.

For the D-curves (2.8), equation (2.11) gives $\operatorname{sgn}(\gamma'_b) = \operatorname{sgn}(\cos(\omega\tau) + b\tau)$. This yields two possible cases.

1. If $\omega \in ((2k-1)\pi, 2k\pi)$, $k \in \mathbb{Z}^+$, then the corresponding D-curves (2.8) satisfy $b > 1/\tau$; consequently, γ'_b is positive in this case. This means that the complex conjugate pair of critical characteristic exponents crosses the imaginary axis from left to right, i.e., two stable exponents become unstable as b is increased.
2. If $\omega \in (2k\pi, (2k+1)\pi)$, $k \in \mathbb{N}$, then the D-curves (2.8) satisfy $b < -1/\tau$; consequently, γ'_b is negative. This means that the complex conjugate pair of critical characteristic exponents crosses the imaginary axis from right to left, i.e., two unstable exponents become stable as b is increased.

Overall, it can be concluded that more and more unstable characteristic exponents appear along the D-curves (2.8) as $|b|$ is increased. Since the half-line $b = 0$ with $a < 0$ is associated with an asymptotically stable ODE, the number of unstable exponents in the region containing this half-line is 0. The number of unstable exponents in the neighboring domains can be given by considering the exponent-crossing directions along the D-curves. The corresponding stability chart with the number of unstable characteristic exponents is presented in Figure 2.1. Stable domains (with 0 unstable exponents) are indicated by gray shading. The limits for the frequency parameter ω along the D-curves are also presented.

The number of unstable characteristic exponents can also be determined using Stepan's formula (1.26) for systems with odd dimension. According to (1.24), the real and the imaginary part of $D(\mathrm{i}\omega)$ define the functions

$$R(\omega) = -a - b\cos(\omega\tau) \,, \quad \omega \in [0, \infty) \,, \tag{2.12}$$

$$S(\omega) = \omega + b\sin(\omega\tau) \,, \quad \omega \in [0, \infty) \,. \tag{2.13}$$

Note that the D-curves (2.7) and (2.8) are given by the equations $R(\omega) = 0$ and $S(\omega) = 0$. The stability analysis can be performed for each domain separated by the D-curves step by step. Consider, for instance, the parameters $a = 0$, $b = -5$ and $\tau = 1$ that are associated with point A within the domain of two unstable exponents (see Figure 2.1). For these parameters, $S(\omega)$ has the zeros $\sigma_1 = 2.5957$ and $\sigma_2 = 0$, and (1.26) gives $N = 2$. The analysis for the other domains can be performed in the

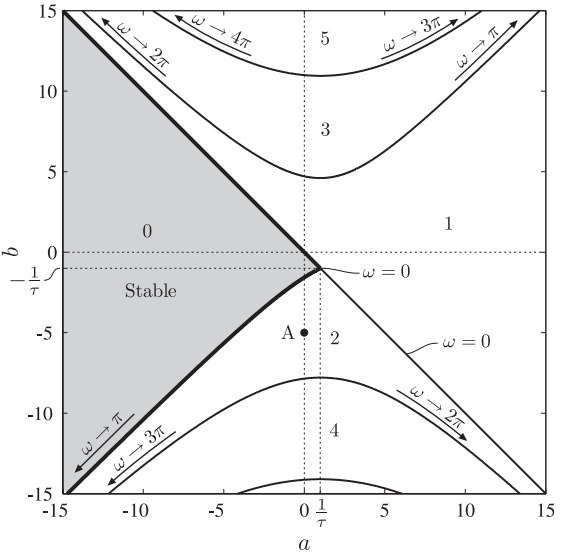

Fig. 2.1 Stability chart with the number of unstable characteristic exponents for (2.1) with $\tau = 1$.

same way, and the number of unstable exponents can be determined for the whole parameter plane (a, b).

2.1.2 The Cushing Equation

The counterpart of (2.1) with distributed delay reads

$$\dot{x}(t) = ax(t) + b \int_{-\sigma}^{0} w(\vartheta) x(t + \vartheta) \, \mathrm{d}\vartheta \, . \tag{2.14}$$

This equation was analyzed by Cushing [60] in relation to population dynamics. If the kernel function is $w(\vartheta) = \delta(\vartheta - \tau)$, $\sigma \le \tau \le 0$, with $\delta(\vartheta)$ being the Dirac delta distribution, then (2.14) gives (2.1). Stability properties of (2.14) with the kernel function $w(\vartheta)$ being the gamma distribution was analyzed in [29, 30, 198]. Here, the stability properties are determined for the kernel function $w(\vartheta) \equiv 1$ (see [18]).

The characteristic function for (2.14) with $w(\vartheta) \equiv 1$ reads

$$D(\lambda) = \lambda - a - b \frac{1 - \mathrm{e}^{-\lambda\sigma}}{\lambda} \, , \quad \lambda \neq 0 \, , \tag{2.15}$$

with the continuous extension at $\lambda = 0$ with

$$D(0) = \lim_{\lambda \to 0} D(\lambda) = -a - b\sigma \,. \tag{2.16}$$

According to the D-subdivision method, substitution of $\lambda = \gamma \pm \mathrm{i}\omega$, $\omega \geq 0$, into $D(\lambda) = 0$ and decomposition into real and imaginary parts gives

$$\text{Re} \;:\quad \gamma - a - b\frac{\gamma - \gamma\,\mathrm{e}^{-\gamma\sigma}\cos(\omega\sigma) + \omega\,\mathrm{e}^{-\gamma\sigma}\sin(\omega\sigma)}{\gamma^2 + \omega^2} = 0 \,, \tag{2.17}$$

$$\text{Im} \;:\quad \omega + b\frac{\omega - \omega\,\mathrm{e}^{-\gamma\sigma}\cos(\omega\sigma) - \gamma\,\mathrm{e}^{-\gamma\sigma}\sin(\omega\sigma)}{\gamma^2 + \omega^2} = 0 \,. \tag{2.18}$$

If $\gamma = 0$, then (2.17) and (2.18) give the D-curves in the parametric form

$$\text{if } \omega = 0 \;:\quad b = -\frac{1}{\sigma}a \,, \tag{2.19}$$

$$\text{if } \omega\tau \neq k\pi \,,\; k \in \mathbb{N} :\quad a = \frac{\omega\sin(\omega\sigma)}{1 - \cos(\omega\sigma)} \,, \quad b = \frac{-\omega^2}{1 - \cos(\omega\sigma)} \,, \tag{2.20}$$

with the corresponding limits for $\omega\sigma = k\pi$, $k \in \mathbb{N}$.

Similarly to the analysis of (2.1), the exponent-crossing direction at the D-curves can be obtained by taking the partial derivatives of (2.17) and (2.18) with respect to b and then setting $\gamma = 0$ and solving the resulting equations for γ'_b. This derivation gives

$$\gamma'_b = \frac{1}{A^2 + B^2}\left(\frac{1 - \cos(\omega\sigma)}{\omega^2}b\sigma + \frac{\sin(\omega\sigma)}{\omega}\right) \,, \tag{2.21}$$

where

$$A = 1 - \frac{1 - \cos(\omega\sigma) - \omega\sigma\sin(\omega\sigma)}{\omega^2}b \,, \tag{2.22}$$

$$B = \frac{\sin(\omega\sigma) - \omega\sigma\cos(\omega\sigma)}{\omega^2}b \,. \tag{2.23}$$

Taking the limit $\omega \to 0$ gives the exponent-crossing direction along the D-curve (2.19) associated with $\omega = 0$ as

$$\gamma'_b = \frac{2\sigma}{b\sigma^2 + 2} \,. \tag{2.24}$$

If $b > -2/\sigma^2$, then γ'_b is positive; consequently, as b is increased, the critical characteristic exponent crosses the imaginary axis from left to right through the origin, i.e., a stable exponent becomes unstable. If $b < -2/\sigma^2$, then γ'_b is negative, and the critical characteristic exponent crosses the imaginary axis in the opposite direction, i.e., an unstable exponent becomes stable as b is increased.

For the D-curves (2.20), equation (2.21) gives

$$\operatorname{sgn}\gamma'_b = \operatorname{sgn}\left(-\sigma + \frac{\sin(\omega\sigma)}{\omega}\right) \,, \tag{2.25}$$

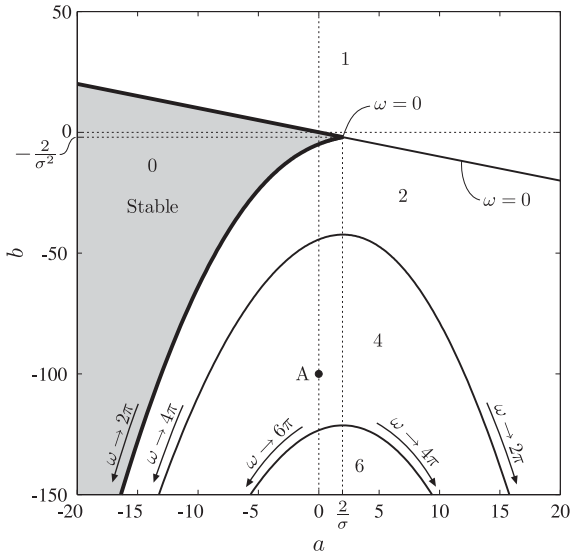

Fig. 2.2 Stability chart with the number of unstable characteristic exponents for (2.14) with $w(\vartheta) \equiv 1, \sigma = 1$.

which is always negative if $\omega \neq 0$. This implies that new pairs of unstable exponents appear at each D-curve given by (2.20) as b is decreased.

Utilizing that the half-line $b = 0$ with $a < 0$ is associated with an asymptotically stable ODE, the number of unstable exponents can be given for each region by considering the exponent-crossing direction at the corresponding D-curves. The stability chart with the number of unstable exponents can be seen in Figure 2.2. Stable domains are indicated by gray shading. The limits for the frequency parameter ω along the D-curves are also presented.

Again, the application of Stepan's formula (1.26) with the functions

$$R(\omega) = -a - b\frac{\sin(\omega\sigma)}{\omega}\,, \quad \omega \in [0, \infty)\,, \tag{2.26}$$

$$S(\omega) = \omega + b\frac{1 - \cos(\omega\sigma)}{\omega}\,, \quad \omega \in [0, \infty)\,, \tag{2.27}$$

defined in (1.24) can also be used to determine the number of unstable characteristic exponents for the individual domains in Figure 2.2. Consider, for instance, the parameters $a = 0$, $b = -100$, and $\sigma = 1$ that are associated with point A within the domain of four unstable exponents. For these parameters, $S(\omega)$ has the zeros $\sigma_1 = 10.823$, $\sigma_2 = 7.3814$, $\sigma_3 = 5.4864$, $\sigma_4 = 0$, and (1.26) gives $N = 4$. The analysis for the other domains can be performed in the same way.

2.2 Delayed Oscillators

A well-known Newtonian example for delayed systems is the damped delayed oscillator described by the scalar DDE

$$\ddot{x}(t) + a_1\dot{x}(t) + a_0 x(t) = b_0\, x(t-\tau)\ . \tag{2.28}$$

Although the stability chart in the parameter plane (a_0, b_0) has a very clear structure (see Figures 2.4 and 2.5), it was first published correctly only in 1966 by Hsu and Bhatt [112]. Since then, this equation has become a basic example for delayed Newtonian problems; see, for instance, [153, 255, 44, 179]. Stability analysis for the generalizations of (2.28) have been considered in detail in [53, 160, 245, 176].

The special case of (2.28) with $b_0 = 0$ is the damped oscillator

$$\ddot{x}(t) + a_1\dot{x}(t) + a_0 x(t) = 0\ . \tag{2.29}$$

The characteristic function (which is a polynomial in this case) reads

$$D(\lambda) = \lambda^2 + a_1\lambda + a_0\ , \tag{2.30}$$

and the characteristic exponents are

$$\lambda_{1,2} = \frac{-a_1 \pm \sqrt{a_1^2 - 4a_0}}{2}\ . \tag{2.31}$$

Substitution of $\lambda = \pm \mathrm{i}\omega$, $\omega \geq 0$, into (2.30) gives the D-curves in the form

$$\text{if } \omega = 0\ :\quad a_0 = 0\ ,\quad a_1 \in \mathbb{R}\ , \tag{2.32}$$

$$\text{if } \omega \neq 0\ :\quad a_1 = 0\ ,\quad a_0 = \omega^2 > 0\ . \tag{2.33}$$

The number of unstable exponents can be determined based on (2.31). The stability properties are presented in Figure 2.3.

Consider now the undamped delayed oscillator

$$\ddot{x}(t) + a_0 x(t) = b_0 x(t-\tau)\ , \tag{2.34}$$

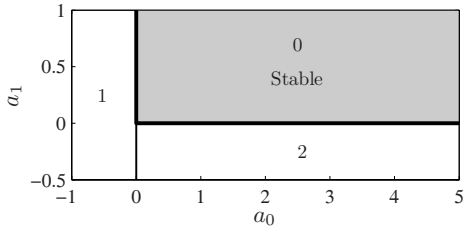

Fig. 2.3 Stability chart with the number of unstable characteristic exponents for the damped oscillator (2.29).

which is a special case of (2.28) with $a_1 = 0$. The corresponding characteristic function is

$$D(\lambda) = \lambda^2 + a_0 - b_0 \mathrm{e}^{-\lambda\tau} \,. \tag{2.35}$$

According to the D-subdivision method, substitution of $\lambda = \gamma \pm \mathrm{i}\omega$, $\omega \geq 0$, into $D(\lambda) = 0$ and decomposition into real and imaginary parts yields

$$\text{Re} : \quad \gamma^2 - \omega^2 + a_0 - b_0 \mathrm{e}^{-\gamma\tau} \cos(\omega\tau) = 0 \,, \tag{2.36}$$

$$\text{Im} : \quad 2\gamma\omega + b_0 \mathrm{e}^{-\gamma\tau} \sin(\omega\tau) = 0 \,. \tag{2.37}$$

If $\gamma = 0$, then (2.36) and (2.37) give the D-curves in the form

$$\text{if } \omega\tau = k\pi \,,\ k \in \mathbb{N} \ : \quad b_0 = (-1)^k a_0 - (-1)^k \left(\frac{k\pi}{\tau}\right)^2 \,, \tag{2.38}$$

$$\text{if } \omega\tau \neq k\pi \,,\ k \in \mathbb{N} : \quad b_0 = 0 \,, \quad a_0 = \omega^2 > 0 \,. \tag{2.39}$$

These D-curves are straight lines in the plane (a_0, b_0) and form a special combination of triangles, shown in Figure 2.4. The D-curve $b_0 = a_0$ given by (2.38) with $k = 0$ is associated with a real critical characteristic exponent $\lambda = 0$. All the other D-curves are associated with the complex conjugate pair of characteristic exponents of the form $\lambda = \pm\mathrm{i}\omega$.

The exponent-crossing direction along the D-curves can be obtained by taking the partial derivatives of (2.36) and (2.37) with respect to b_0 and substituting the D-curves (2.38), (2.39), and $\gamma = 0$. For the D-curves (2.38), this analysis gives

$$\gamma'_{b_0} = \frac{b_0\tau}{b_0^2\tau^2 + 4\omega^2} \,, \tag{2.40}$$

that is, γ'_{b_0} is positive for $b_0 > 0$ and negative for $b_0 < 0$. This means that new unstable exponents appear as these D-curves are crossed with increasing $|b_0|$. Along the D-curve $a_0 = b_0$ associated with $k = 0$ in (2.38), a real characteristic exponent becomes unstable as $|b_0|$ is increased, while at the other D-curves associated with $k > 0$, a pair of complex characteristic exponents crosses the imaginary axis from left to right for increasing $|b_0|$.

The analysis for the D-curve (2.39) gives

$$\gamma'_{b_0} = \frac{-\sin(\omega\tau)}{2\omega} \tag{2.41}$$

with $\omega = \sqrt{a_0}$. In this case, the sign of γ'_{b_0} can be given as

$$\gamma'_{b_0} < 0 \qquad \text{if} \quad \left(\frac{2m\pi}{\tau}\right)^2 < a_0 < \left(\frac{(2m+1)\pi}{\tau}\right)^2 \,, \quad m \in \mathbb{N} \,, \tag{2.42}$$

$$\gamma'_{b_0} > 0 \qquad \text{if} \quad \left(\frac{(2m+1)\pi}{\tau}\right)^2 < a_0 < \left(\frac{(2m+2)\pi}{\tau}\right)^2 \,, \quad m \in \mathbb{N} \,. \tag{2.43}$$

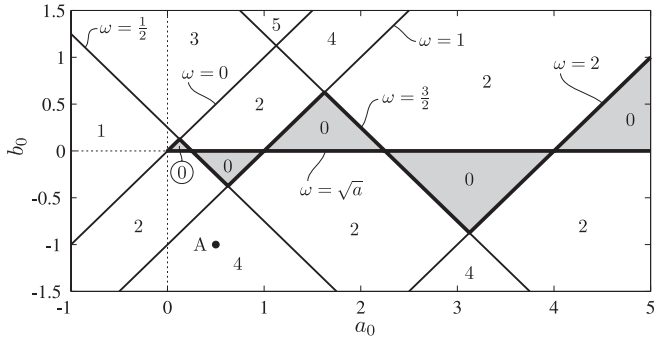

Fig. 2.4 Hsu–Bhatt stability chart with the number of unstable characteristic exponents for (2.34) with $\tau = 2\pi$.

This means that a pair of complex characteristic exponents becomes unstable as the line $b_0 = 0$ with $a_0 > 0$ is crossed from inside the triangles (see Figure 2.4).

Since the half-line $b_0 = 0$ with $a_0 < 0$ is associated with an ODE with one unstable characteristic exponent (see Figure 2.3), the number of unstable exponents can be given for all regions by considering the exponent-crossing directions along the corresponding D-curves. The stability chart with the number of unstable characteristic exponents is presented in Figure 2.4. Stable domains are indicated by gray shading. The frequency parameter ω along the stability boundaries is also presented.

The number of unstable characteristic exponents can also be determined using Stepan's formula (1.25) for systems with even dimension. According to (1.24), the real and the imaginary part of $D(\mathrm{i}\omega)$ define the functions

$$R(\omega) = -\omega^2 + a_0 - b_0 \cos(\omega\tau) , \quad \omega \in [0, \infty) , \tag{2.44}$$

$$S(\omega) = b_0 \sin(\omega\tau) , \quad \omega \in [0, \infty) . \tag{2.45}$$

For this analysis, (1.25) should be applied for some fixed parameters associated with the individual domains in Figure 2.4. For instance, the parameters $a_0 = 0.5$, $b_0 = -1$, and $\tau = 2\pi$ are associated with point A within the domain of four unstable exponents. For these parameters, $R(\omega)$ has the zeros $\rho_1 = 1.1161$, $\rho_2 = 0.7631$, $\rho_3 = 0.3156$, and (1.25) gives $N = 4$. All the other domains can be analyzed in a similar way.

Consider now the damped and delayed case, i.e., (2.28) with $a_1 \neq 0$ and $b_0 \neq 0$. The corresponding characteristic function is

$$D(\lambda) = \lambda^2 + a_1\lambda + a_0 - b_0 \mathrm{e}^{-\lambda\tau} . \tag{2.46}$$

Substitution of $\lambda = \pm\mathrm{i}\omega$, $\omega \geq 0$, into $D(\lambda) = 0$ gives the D-curves in the form

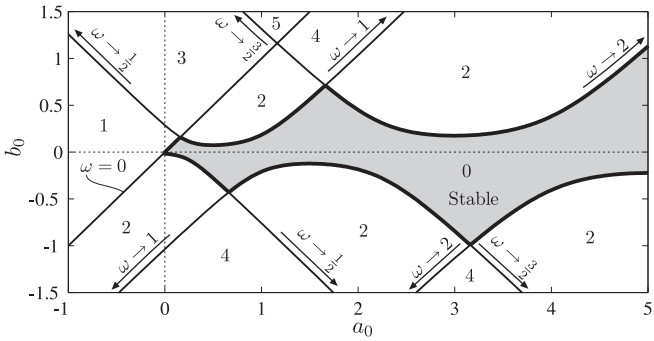

Fig. 2.5 Hsu–Bhatt stability chart with the number of unstable characteristic exponents for (2.28) with $a_1 = 0.1$ and $\tau = 2\pi$.

$$\text{if } \omega = 0 \ : \quad b_0 = a_0 \ , \tag{2.47}$$

$$\text{if } \omega\tau \neq k\pi \ , \ k \in \mathbb{N} : \quad a_0 = \omega^2 + \frac{a_1 \omega \cos(\omega\tau)}{\sin(\omega\tau)} \ , \quad b_0 = \frac{-a_1\omega}{\sin(\omega\tau)} \ . \tag{2.48}$$

The number of unstable exponents for the domains bounded by (2.47) and (2.48) can be determined based on continuous dependence of the characteristic exponents on the system parameters. For this purpose, the stability chart for the case $a_1 = 0$ in Figure 2.4 can be used as a reference. The corresponding stability chart is shown in Figure 2.5. Stable domains are indicated by gray shading. The limits for the frequency parameter ω along the stability boundaries are also presented.

2.3 Stabilization with Feedback Delay

Stabilization of a one-degree-of-freedom Newtonian system about an unstable equilibrium by a proportional-derivative controller in the presence of feedback delay is described by the equation

$$\ddot{x}(t) + a_0 x(t) = -k_\mathrm{p} x(t-\tau) - k_\mathrm{d} \dot{x}(t-\tau) \ , \tag{2.49}$$

where $a_0 < 0$ is the negative stiffness, k_p is the proportional gain, k_d is the derivative gain, and τ is the feedback delay. This equation corresponds to the general second-order delayed system

$$\ddot{x}(t) + a_1 \dot{x}(t) + a_0 x(t) = b_0 x(t-\tau) + b_1 \dot{x}(t-\tau) \tag{2.50}$$

with $b_0 = -k_\mathrm{p}$, $b_1 = -k_\mathrm{d}$, and $a_1 = 0$. Equation (2.49) is a frequently cited example in dynamics and control theory [255, 243, 166], and it is also relevant to human balancing problems [263, 260, 190].

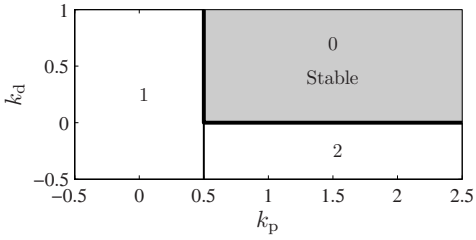

Fig. 2.6 Stability chart with the number of unstable characteristic exponents for (2.51) with $a_0 = -0.5$.

If $a_0 < 0$ and $k_p = 0$, $k_d = 0$, then the system is unstable with the characteristic exponents $\lambda_{1,2} = \pm\sqrt{-a_0}$, i.e., the number of unstable exponents is 1.

If the feedback delay is zero, then the governing equation reads

$$\ddot{x}(t) + a_0\, x(t) = -k_p\, x(t) - k_d\, \dot{x}(t)\,, \tag{2.51}$$

which is equivalent to the well-known damped oscillator (2.29) with some appropriate parameter transformations. In this case, the D-curves can be given in the form

$$\text{if } \omega = 0 \;:\quad k_p = a_0\,, \quad k_d \in \mathbb{R}\,, \tag{2.52}$$

$$\text{if } \omega \neq 0 \;:\quad k_d = 0\,, \quad k_p = -a_0 + \omega^2 > -a_0\,, \tag{2.53}$$

where ω is the imaginary part of the critical characteristic exponent. The stability chart with the number of unstable exponents is presented in Figure 2.6. This chart shows that if the feedback delay τ is 0, then the unstable system can be stabilized by control gains $k_p > -a_0$ and $k_d > 0$.

Consider now (2.49) with $\tau > 0$. The corresponding characteristic function reads

$$D(\lambda) = \lambda^2 + a_0 + k_p \mathrm{e}^{-\lambda\tau} + k_d \lambda \mathrm{e}^{-\lambda\tau}\,. \tag{2.54}$$

According to the D-subdivision method, substitution of $\lambda = \gamma \pm \mathrm{i}\omega$, $\omega \geq 0$, into $D(\lambda) = 0$ and decomposition into real and imaginary parts gives

$$\text{Re}\;:\quad \gamma^2 - \omega^2 + a_0 + k_p \mathrm{e}^{-\gamma\tau}\cos(\omega\tau) + k_d\gamma\,\mathrm{e}^{-\gamma\tau}\cos(\omega\tau) + k_d\omega \mathrm{e}^{-\gamma\tau}\sin(\omega\tau) = 0\,, \tag{2.55}$$

$$\text{Im}\;:\quad 2\gamma\omega - k_p \mathrm{e}^{-\gamma\tau}\sin(\omega\tau) + k_d\omega \mathrm{e}^{-\gamma\tau}\cos(\omega\tau) - k_d\gamma\,\mathrm{e}^{-\gamma\tau}\sin(\omega\tau) = 0\,. \tag{2.56}$$

The case $\gamma = 0$ gives the D-curves in the form

$$\text{if } \omega = 0 \;:\quad k_p = -a_0\,, \quad k_d \in \mathbb{R}\,, \tag{2.57}$$

$$\text{if } \omega \neq 0 \;:\quad k_p = (\omega^2 - a_0)\cos(\omega\tau)\,, \quad k_d = \frac{\omega^2 - a_0}{\omega}\sin(\omega\tau)\,. \tag{2.58}$$

The D-curve $k_p = -a_0$ given by (2.57) is associated with a real critical characteristic exponent $\lambda = 0$. The D-curve given by (2.58) is associated with a complex conjugate

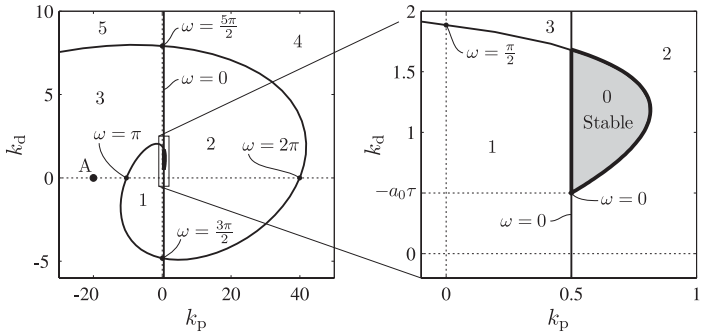

Fig. 2.7 Stability chart with the number of unstable characteristic exponents for (2.49) with $a_0 = -0.5$ and $\tau = 1$.

pair of characteristic exponents of the form $\lambda = \pm i\omega$. For a fixed a_0, these curves cut the parameter plane (k_p, k_d) into infinitely many domains (see Figure 2.7).

The exponent-crossing direction along the D-curve $k_p = -a_0$ can be obtained by taking the partial derivatives of (2.55) and (2.56) with respect to k_p and substituting $\gamma = 0$, $\omega = 0$, and $k_p = -a_0$. This derivation gives

$$\gamma'_{k_p} = -\frac{1}{a_0\tau + k_d} , \tag{2.59}$$

that is, γ'_{k_p} is positive for $k_d < -a_0\tau$ and negative for $k_d > -a_0\tau$. If the line $k_p = -a_0$ is crossed from left to right with $k_d > -a_0\tau$, then a real characteristic exponent becomes stable. If $k_d < -a_0\tau$, then a real exponent becomes unstable as the line $k_p = -a_0$ is crossed from left to right. Since the parameter point $(k_p, k_d) = (0, 0)$ corresponds to an ODE with one unstable characteristic exponent, the number of unstable exponents can be given for all the domains in the parameter plane (k_p, k_d) by considering the exponent-crossing directions along the D-curve $k_p = -a_0$. The corresponding stability chart with the number of unstable exponents is presented in Figure 2.7. The stable domain is indicated by gray shading. Some specific values of the frequency parameter ω along the stability boundaries are also presented.

The number of unstable exponents can also be determined using Stepan's formula (1.25) with the functions

$$R(\omega) = -\omega^2 + a_0 + k_p \cos(\omega\tau) + k_d\omega \sin(\omega\tau) , \quad \omega \in [0, \infty) , \tag{2.60}$$

$$S(\omega) = -k_p \sin(\omega\tau) - k_d\omega \cos(\omega\tau) , \quad \omega \in [0, \infty) . \tag{2.61}$$

For instance, the parameters $a_0 = -0.5$, $\tau = 1$, $k_p = -20$, and $k_d = 0$ are associated with point A within the domain of three unstable exponents in Figure 2.7. For these parameters, $R(\omega)$ has the zeros $\rho_1 = 3.844$ and $\rho_2 = 1.750$, and (1.25) gives $N = 3$. All the other domains can be analyzed in a similar way.

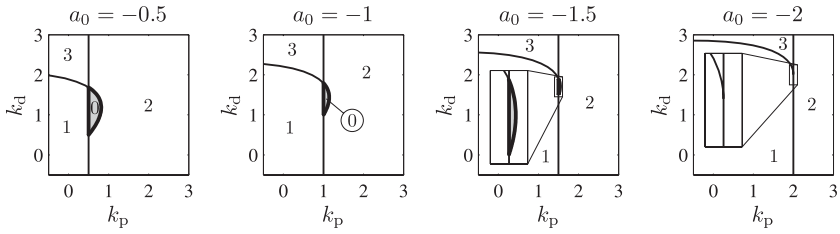

Fig. 2.8 Stability charts with the number of unstable characteristic exponents for (2.49) with $\tau = 1$ for different system parameters a_0.

Figure 2.8 shows the stability charts for different system parameters a_0. It can be observed that as a_0 is decreased, the stable domain shrinks, and at $a_0 = -2$, it completely disappears. This can easily be seen by the analysis of the tangent of the parametric curve (2.58) at $\omega = 0$. A long but straightforward analysis gives

$$\lim_{\omega\to 0} \frac{\mathrm{d}k_\mathrm{d}}{\mathrm{d}k_\mathrm{p}} = \lim_{\omega\to 0} \frac{\dfrac{\mathrm{d}k_\mathrm{d}}{\mathrm{d}\omega}}{\dfrac{\mathrm{d}k_\mathrm{p}}{\mathrm{d}\omega}} = \frac{a_0\tau^3 + 6\tau}{3a_0\tau^2 + 6} \,. \tag{2.62}$$

The tangent is vertical if $3a_0\tau^2 + 6 = 0$, which gives the critical value $a_{0,\mathrm{crit}} = -2/\tau^2$. If $a_0 < a_{0,\mathrm{crit}}$, then (2.49) is unstable for any k_p and k_d. For the case $\tau = 1$ in Figure 2.8, the critical value is $a_{0,\mathrm{crit}} = -2$.

The same phenomenon is often considered from the delay point of view: for a fixed system parameter $a_0 < 0$, there exists a critical delay $\tau_\mathrm{crit} = \sqrt{-2/a_0}$. If the feedback delay is larger than τ_crit, then the system is unstable for all combinations of k_p and k_d.

2.4 Delayed Mathieu Equation

A paradigm for time-delayed and time-periodic systems is the damped and delayed Mathieu equation

$$\ddot{x}(t) + a_1\dot{x}(t) + (\delta + \varepsilon\cos t)\, x(t) = b_0 x(t-\tau) \,. \tag{2.63}$$

This equation combines the phenomenon of parametric forcing with the effect of time delay. Consequently, stability analysis can be performed based on the Floquet theory of DDEs [97, 100]. Here, the special resonant case will be investigated, when $\tau = 2\pi$, i.e., the time delay is just equal to the principal period, and the stability charts will be constructed by Hill's infinite determinant method.

2.4.1 Special Cases

The special case $b_0 = 0$ gives the classical damped Mathieu equation

$$\ddot{x}(t) + a_1\dot{x}(t) + (\delta + \varepsilon\cos t)\,x(t) = 0\,. \tag{2.64}$$

This equation (with $a_1 = 0$) was first discussed by Mathieu [183] in relation to the vibrations of an elliptic membrane, but it is also known as the model equation for the small oscillations of a pendulum under parametric forcing (i.e., with periodically vibrating suspension point) around its upper and the lower equilibria [265, 146, 170]. The stability chart in the plane (δ, ε), the so-called Ince–Strutt diagram, was published by van der Pol and Strutt [286] in 1928, but the functions of the stability boundaries were already given in the textbook of Ince [116] in 1926.

According to the Floquet theory, the stability of (2.64) is determined by the eigenvalues of the monodromy matrix. As was mentioned in Section 1.2, this matrix has, in general, no closed-form representation, but there exist several methods to give a sufficiently accurate approximation (see, for instance, [205] for an overview). Here the piecewise constant approximation of the periodic matrix is used according to [111]. Equation (2.64) can be transformed into the state-space form

$$\dot{\mathbf{y}}(t) = \mathbf{A}(t)\mathbf{y}(t), \quad \mathbf{A}(t) = \mathbf{A}(t+T)\,, \tag{2.65}$$

with

$$\mathbf{y}(t) = \begin{pmatrix} x(t) \\ \dot{x}(t) \end{pmatrix}\,, \quad \mathbf{A}(t) = \begin{pmatrix} 0 & 1 \\ -(\delta + \varepsilon\cos t) & -a_1 \end{pmatrix}\,. \tag{2.66}$$

After piecewise constant approximation of the coefficient matrix according to (1.9), the Floquet transition matrix can be approximated as

$$\mathbf{\Phi}(T) \approx \tilde{\mathbf{\Phi}}(T) = \mathrm{e}^{\mathbf{A}_{p-1}h}\,\mathrm{e}^{\mathbf{A}_{p-2}h}\,\cdots\,\mathrm{e}^{\mathbf{A}_0 h}\,, \tag{2.67}$$

where $h = T/p$ is the length of the discretization step, with p being an integer, and $\mathbf{A}_i$ is the average of the time-periodic matrix $\mathbf{A}(t)$ over the ith discretization step defined by (1.8). The system is asymptotically stable if the eigenvalues of $\mathbf{\Phi}(T)$ (i.e., the characteristic multipliers) have modulus less than one. The stability chart can be constructed by point-by-point evaluation of the critical eigenvalues over a fixed-sized grid of parameters δ and ε. The corresponding stability chart obtained by $p = 20$ is shown in Figure 2.9 for different damping parameters a_1.

According to Liouville's formula [83], the determinant of the monodromy matrix can be given as

$$\det\mathbf{\Phi}(T) = \exp\left(\int_0^T \mathrm{Tr}\,\mathbf{A}(t)\,\mathrm{d}t\right) = \exp\left(\int_0^T -a_1\,\mathrm{d}t\right) = \mathrm{e}^{-a_1 T}\,. \tag{2.68}$$

Since $\mathbf{A}$ is a 2×2 matrix, $\det\mathbf{\Phi}(T) = \mu_1\mu_2$, where μ_1 and μ_2 are the two characteristic multipliers with $|\mu_1| \geq |\mu_2|$. The location of the multipliers in the complex plane can be characterized as follows.

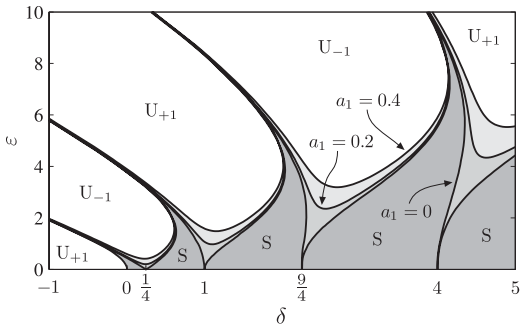

Fig. 2.9 Ince–Strutt [116, 286] stability chart for (2.64). S indicates stable domains, U_{+1} and U_{-1} indiciate unstable domains with critical characteristic multipliers $\mu_1 > 1$ and $\mu_1 < -1$, respectively. Stability boundaries are presented for $a_1 = 0$, 0.2, and 0.4.

1. If $a_1 < 0$, then $\mu_1\mu_2 > 1$, i.e., at least one of the characteristic multipliers has modulus larger than 1. Consequently, the Mathieu equation (2.64) with negative damping a_1 is always unstable.
2. If $a_1 = 0$, then $\mu_1\mu_2 = 1$. In this case, the system is stable in the Lyapunov sense if $|\mu_1| = 1$ and $|\mu_2| = 1$; otherwise, the system is unstable with $|\mu_1| > 1$ and $|\mu_2| < 1$. Asymptotic stability does not occur in this case.
3. If $a_1 > 0$, then $\mu_1\mu_2 < 1$. In this case, one of the characteristic multipliers is always located within the unit circle. The system can be asymptotically stable with $|\mu_2| \le |\mu_1| < 1$.

The above cases show that both characteristic multipliers can never cross the unit circle at the same time. Consequently, in the damped Mathieu equation (2.64), only cyclic-fold or period-doubling (flip) bifurcations may occur, and secondary Hopf bifurcation does not arise. In Figure 2.9, stability curves bounding the unstable domains indicated by U_{+1} represent cyclic-fold bifurcations, while the curves bounding the domains indicated by U_{-1} represent period-doubling bifurcations.

The special case $\varepsilon = 0$ of (2.63) gives the damped and delayed oscillator (2.28) with $a_0 = \delta$ discussed in Section 2.2. The corresponding stability charts can be seen in Figure 2.4 for $a_1 = 0$, $\tau = 2\pi$ and in Figure 2.5 for $a_1 = 0.1$, $\tau = 2\pi$. These charts were published first by Hsu and Bhatt [112] in 1966.

2.4.2 D-curves

First, the D-curves for the undamped system in the plane (δ, b_0) are determined by Hill's infinite determinant method. The undamped case of (2.63) with $a_1 = 0$ reads

$$\ddot{x}(t) + (\delta + \varepsilon \cos t)\, x(t) = b_0 x(t - 2\pi)\ . \tag{2.69}$$

The corresponding stability chart in the space of system parameters δ, b_0, and ε was published by Insperger and Stepan [124] in 2002. This chart combines the Ince–Strutt stability chart of the Mathieu equation (shown in Figure 2.9) and the Hsu–Bhatt stability chart of the delayed oscillator (shown in Figure 2.4).

The main point in the construction of the stability boundaries for (2.69) is that the points where the lines of slope ± 1 intersect the line $b_0 = 0$ in the Hsu–Bhatt stability chart in Figure 2.4 are $a_0 = 0, 1/4, 1, 9/4, \ldots$, which coincide with the points where the unstable tongues in the Ince–Strutt stability chart in Figure 2.9 open on the δ-axis for $\varepsilon = 0$. In the subsequent analysis, this property will be used to show how the stable triangles in the plane (a_0, b_0) in Figure 2.4 change for $\varepsilon > 0$. The investigation is based on the following theorems of the Floquet theory of DDEs (see, e.g., [83]):

- The trivial solution of (2.69) is asymptotically stable if and only if all the (infinitely many) characteristic multipliers have modulus less than one;
- $\mu = \mathrm{e}^{\lambda T}$ is a characteristic multiplier of (2.69) if and only if there exists a non-trivial solution in the form $x(t) = p(t)\mathrm{e}^{\lambda t}$, where $p(t) = p(t+T)$, with T being the principal period (in this case $T = 2\pi$).

This implies the application of the trial solution in the form

$$x(t) = p(t)\mathrm{e}^{\lambda t} + \bar{p}(t)\mathrm{e}^{\bar{\lambda} t} , \tag{2.70}$$

where $p(t) = p(t + 2\pi)$ is a periodic function and bar denotes complex conjugate. Note that λ is a characteristic exponent, that is, if $\mathrm{Re}\,\lambda < 0$, then the trivial solution $x(t) \equiv 0$ is asymptotically stable.

According to Hahn [96], equation (2.69) may have solutions of the form $t^k p(t)\mathrm{e}^{\lambda t}$, $k \in \mathbb{Z}^+$, in critical cases. Consequently, if $|\mu| = 1$, i.e., $\mathrm{Re}\,\lambda = 0$, then the solution $p(t)\mathrm{e}^{0t}$ is stable in the Lyapunov sense, but the solutions $t^k p(t)\mathrm{e}^{0t}$ are unstable. This case has no importance here, since it may arise only at certain special points of the stability boundaries, while in the present investigation, the domains of asymptotic stability are determined.

Expand the periodic function $p(t)$ in (2.70) into a Fourier series to obtain

$$x(t) = \left(\sum_{k=0}^{\infty} A_k \mathrm{e}^{\mathrm{i}kt} + B_k \mathrm{e}^{-\mathrm{i}kt} \right) \mathrm{e}^{\lambda t} + \left(\sum_{k=0}^{\infty} \bar{A}_k \mathrm{e}^{-\mathrm{i}kt} + \bar{B}_k \mathrm{e}^{\mathrm{i}kt} \right) \mathrm{e}^{\bar{\lambda} t} . \tag{2.71}$$

Using trigonometric transformations, (2.71) can be transformed to

$$x(t) = \sum_{k=-\infty}^{\infty} C_k \mathrm{e}^{(\lambda + \mathrm{i}k)t} + \bar{C}_k \mathrm{e}^{(\bar{\lambda} - \mathrm{i}k)t} . \tag{2.72}$$

Substitution into (2.69) and balancing of the harmonics $\mathrm{e}^{(\lambda+\mathrm{i}k)t}$ and $\mathrm{e}^{(\bar{\lambda}-\mathrm{i}k)t}$ yields two systems of equations for the coefficients C_k and $\bar{C}_k$:

$$\frac{\varepsilon}{2}C_{k-1} + c_k C_k + \frac{\varepsilon}{2}C_{k+1} = 0\,, \quad k \in \mathbb{Z}\,, \tag{2.73a}$$

$$\frac{\varepsilon}{2}\bar{C}_{k-1} + \bar{c}_k \bar{C}_k + \frac{\varepsilon}{2}\bar{C}_{k+1} = 0\,, \quad k \in \mathbb{Z}\,, \tag{2.73b}$$

where

$$c_k = \delta + (\lambda + \mathrm{i}k)^2 - b_0 \mathrm{e}^{-2\pi(\lambda+\mathrm{i}k)}\,. \tag{2.74}$$

As follows from the Floquet theory, (2.73a) and (2.73b) are satisfied if and only if λ is a characteristic exponent. Since (2.73a) and (2.73b) are equivalent, only (2.73a) will be analyzed. There is a nontrivial solution of system (2.73a) if the number zero is an eigenvalue of the so-called Hill's infinite matrix

$$\mathcal{H}(\lambda) = \begin{pmatrix} \ddots & \ddots & \ddots & \ddots & & & \\ \ddots & \varepsilon/2 & c_{-1} & \varepsilon/2 & 0 & & \\ & 0 & \varepsilon/2 & c_0 & \varepsilon/2 & 0 & \\ & & 0 & \varepsilon/2 & c_1 & \varepsilon/2 & \ddots \\ & & & \ddots & \ddots & \ddots & \ddots \end{pmatrix}. \tag{2.75}$$

This matrix represents an unbounded linear operator $\mathcal{H} : l_2^{\mathbb{Z}} \to l_2^{\mathbb{Z}}$. Here, $l_2^{\mathbb{Z}}$ is the Hilbert space of the complex sequences $(\ldots, z_{-1}, z_0, z_1, \ldots)$ with $\sum_{k=-\infty}^{\infty} |z_k|^2 < \infty$. As is the case for (unbounded) linear operators with compact resolvents, the spectrum of $\mathcal{H}$ consist of a countable number of eigenvalues. All of these eigenvalues are of finite multiplicity. The number zero is an eigenvalue of $\mathcal{H}$ if and only if

$$\operatorname{Ker} \mathcal{H}(\lambda) \neq \{0\}\,. \tag{2.76}$$

Formula (2.76) can be treated as the characteristic equation of (2.69), since its roots are the characteristic exponents. This is a reformulation of (1.37) with $\mu = \exp(2\pi\lambda)$.

In order to carry out calculations, only the truncated system of equations with $k = -N, \ldots, N$ is considered. This reduces the infinite eigenvalue problem of operator $\mathcal{H}$ to the calculation of a finite determinant

$$D(\lambda) = \det \begin{pmatrix} c_{-N} & \varepsilon/2 & & & \\ \varepsilon/2 & c_{-N+1} & \varepsilon/2 & & \\ & \ddots & \ddots & \ddots & \\ & & \varepsilon/2 & c_{N-1} & \varepsilon/2 \\ & & & \varepsilon/2 & c_N \end{pmatrix}. \tag{2.77}$$

Although this truncation seems to be a rough approximation, it still has a sound mathematical basis (see [184, 63]). This approximation is just the same as the one applied during the construction of the Ince–Strutt diagram using Hill's method. The equation $D(\lambda) = 0$ can therefore be considered an approximate characteristic equation. In what follows, first, the D-curves will be constructed for $N \to \infty$; then, in Section 2.4.3, the domains of stability will be determined.

According to the D-subdivision method, the substitution of $\lambda = \pm \mathrm{i}\omega$, $\omega \geq 0$, into $D(\lambda) = 0$ gives an implicit form for the approximate D-curves (or D-surfaces) of (2.69) in the parameter space $(\delta, b_0, \varepsilon)$ with the frequency parameter ω. In this case, the diagonal elements in (2.77) read

$$c_k = \delta - (\omega + k)^2 - b_0 \mathrm{e}^{-\mathrm{i}2\pi\omega} , \qquad k = -N, \ldots, N . \tag{2.78}$$

Note that the imaginary part of c_k does not depend on k:

$$\operatorname{Im} c_k = b_0 \sin(2\pi\omega) , \qquad k = -N, \ldots, N . \tag{2.79}$$

It can be seen that $\operatorname{Im} c_k = 0$ if and only if either $\omega = j/2$ with $j = 0, 1, \ldots$, or $b_0 = 0$, which gives the classical Mathieu equation. Now the cases $\omega \neq j/2$ and $\omega = j/2$ with $j = 0, 1, \ldots$ are investigated separately.

Case $\omega \neq j/2, \quad j = 0, 1, \ldots$

In this case, $\operatorname{Im} c_k \neq 0$ for any k (if $b_0 \neq 0$), as follows from (2.79). The Gaussian elimination algorithm can be applied for the tridiagonal matrix in (2.77) to transform it into an upper triangular matrix having the elements d_k on the main diagonal. Clearly, $d_{-N} = c_{-N} \neq 0$. In the $(N + k)$th step of the Gaussian elimination process, Hill's matrix assumes the form

$$\begin{pmatrix}
d_{-N} & \varepsilon/2 & 0 & \cdots & & & & & \\
 & \ddots & \ddots & \ddots & & & & & \\
\cdots & 0 & d_{k-1} & \varepsilon/2 & 0 & \cdots & & & \\
 & \cdots & 0 & d_k & \varepsilon/2 & 0 & \cdots & & \\
 & \cdots & 0 & \varepsilon/2 & c_{k+1} & \varepsilon/2 & 0 & \cdots & \\
 & & \cdots & 0 & \varepsilon/2 & c_{k+2} & \varepsilon/2 & 0 & \cdots \\
 & & & & \ddots & \ddots & \ddots & \ddots & \ddots
\end{pmatrix} . \tag{2.80}$$

Let us suppose that $\operatorname{sgn}(\operatorname{Im} d_k) = \operatorname{sgn}(\operatorname{Im} c_k)$ for some k. Since $\operatorname{Im} c_k \neq 0$, this means that $\operatorname{Im} d_k \neq 0$, i.e., $|d_k| \neq 0$. Thus, the subsequent elimination of $\varepsilon/2$ to the left from c_{k+1} leads to

$$d_{k+1} = c_{k+1} - \frac{\varepsilon^2}{4 d_k} = \left(\operatorname{Re} c_{k+1} - \frac{\varepsilon^2 \operatorname{Re} d_k}{4 |d_k|^2} \right) + \mathrm{i} \left(\operatorname{Im} c_{k+1} + \frac{\varepsilon^2 \operatorname{Im} d_k}{4 |d_k|^2} \right) . \tag{2.81}$$

Consequently,

$$\operatorname{sgn}(\operatorname{Im} d_{k+1}) = \operatorname{sgn} \left(\operatorname{Im} c_{k+1} + \left(\frac{\varepsilon}{2 |d_k|} \right)^2 \operatorname{Im} d_k \right) = \operatorname{sgn}(\operatorname{Im} d_k) = \operatorname{sgn}(\operatorname{Im} c_k) \neq 0 . \tag{2.82}$$

Since $\operatorname{Im} d_{-N} = \operatorname{Im} c_{-N} = b \sin(2\pi\omega) \neq 0$, we have $\operatorname{Im} d_k \neq 0$, that is, $|d_k| \neq 0$ is true by induction.

The determinant of Hill's matrix can be calculated as the product of the diagonal elements of the upper triangular matrix. Hence,

$$D(\mathrm{i}\omega) = \prod_{k=-N}^{N} d_k \neq 0 \,, \tag{2.83}$$

that is, the determinant (2.77) is never zero if $\lambda = \mathrm{i}\omega$ with $\omega \neq j/2$, $j = 0, 1, \ldots$. This means that there is no nontrivial solution of system (2.73a), and there are no stability boundary curves in this case.

Case $\omega = j/2, \quad j = 0, 1, \ldots$

In this case, the diagonal elements in (2.77) are real:

$$c_k = \delta - \left(k + \tfrac{1}{2}j\right)^2 - b_0(-1)^j \,. \tag{2.84}$$

If j is even, that is, $j = 2h$, $h = 0, 1, \ldots$, then $\lambda = \mathrm{i}h$, and the corresponding characteristic multiplier is

$$\mu = \mathrm{e}^{\mathrm{i}h2\pi} = \mathrm{e}^{\mathrm{i}2\pi} = 1 \,. \tag{2.85}$$

In this case, $c_k = \delta - b_0 - (k+h)^2$, and $D(\lambda) = 0$ gives the relation $f_{+1}(\delta - b_0, \varepsilon) = 0$ for the D-curves. For the case $b_0 = 0$, the relation $f_{+1}(\delta, \varepsilon) = 0$ serves as the U_{+1} D-curves of the classical Mathieu equation defined in the form $\delta = g_{+1}(\varepsilon)$. This means that the D-curves exist for the $b_0 \neq 0$ case, too, in the form

$$\delta - b_0 = g_{+1}(\varepsilon) \,. \tag{2.86}$$

In the plane (δ, b_0), these are lines of slope $+1$ (shown as continuous lines in Figure 2.10). Along these D-curves, there exists a characteristic multiplier $\mu = +1$ representing cyclic-fold bifurcation, and equation (2.69) has a periodic solution of period 2π.

If j is odd, that is, $j = 2h + 1$, $h = 0, 1, \ldots$, then $\lambda = \mathrm{i}(h + 1/2)$, and the corresponding characteristic multiplier is

$$\mu = \mathrm{e}^{\mathrm{i}(h+1/2)2\pi} = \mathrm{e}^{\mathrm{i}\pi} = -1 \,. \tag{2.87}$$

In this case, $c_k = \delta + b_0 - (k + h + 1/2)^2$, and $D(\lambda) = 0$ implies the D-curve relation $f_{-1}(\delta + b_0, \varepsilon) = 0$. For the same reason as above, the D-curves exist again in the form

$$\delta + b_0 = g_{-1}(\varepsilon) \,, \tag{2.88}$$

where $\delta = g_{-1}(\varepsilon)$ gives the U_{-1} D-curves of the classical Mathieu equation. In the parameter plane (δ, b_0), these D-curves are lines of slope -1 (shown as dashed lines in Figure 2.10). Along these D-curves, there exists a characteristic multiplier $\mu = -1$ representing a period-doubling (flip) bifurcation, and equation (2.69) has a nontrivial periodic solution of period 4π.

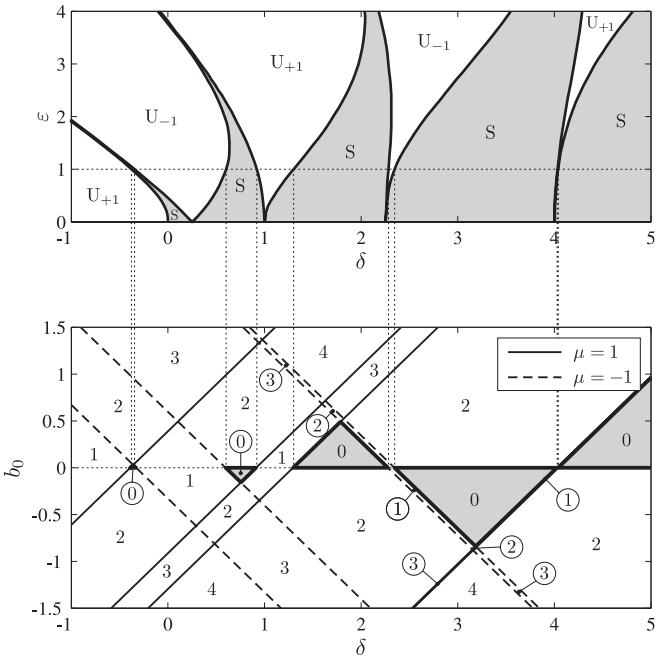

Fig. 2.10 Stability chart with the number of unstable characteristic multipliers for the delayed Mathieu equation (2.69) with $\varepsilon = 1$.

The above analysis showed that the D-curves are straight lines in the plane (δ, b_0) with slopes $+1$, -1 and 0. For varying parameter ε, the lines of slope $+1$ and -1 pass along the stability boundaries of the Ince–Strutt diagram. As mentioned before, these charts are approximate to the same extent as the Ince–Strutt diagram, and the appearance of the delay in the Mathieu equation does not require any further approximation in the stability analysis. The construction of the D-curves in the plane (δ, b_0) for $\varepsilon = 1$ is demonstrated in Figure 2.10. The stability of the domains bounded by the D-curves is determined in the next section.

2.4.3 The Number of Unstable Characteristic Multipliers

The stability of the individual domains separated by the D-curves (2.86) and (2.88) can be determined based on the continuous dependence of the characteristic multipliers on the system parameters. The special case $\varepsilon = 0$ can be treated as a reference: the domains attached to the stable triangles of the Hsu–Bhatt chart (see Figure 2.4) are associated with zero unstable characteristic multipliers. Similarly, some unstable

domains can also be identified in this way, and the number of unstable characteristic multipliers can be given based on the case $\varepsilon = 0$. There are, however, some new domains that are not directly connected to any domains of the Hsu–Bhatt chart. The stability of these domains can be determined by the exponent-crossing direction, i.e., by the analysis of the sign of the partial derivative of $\mathrm{Re}\,\lambda$ with respect to parameter b_0 along the D-curves.

A recursive form for the calculation of the tridiagonal upper left subdeterminants in equation (2.77) can be given as

$$D_{-N} = c_{-N}\,, \tag{2.89}$$

$$D_{-N+1} = c_{-N}c_{-N+1} - \frac{\varepsilon^2}{4}\,, \tag{2.90}$$

$$D_k = c_k D_{k-1} - \frac{\varepsilon^2}{4} D_{k-2}\,, \quad k = -N+2, \ldots, N\,. \tag{2.91}$$

Let us denote the partial derivative with respect to b_0 by a prime ($\square' = \partial\square/\partial b_0$) and the substitution of $\lambda = \mathrm{i}j/2$ by a hat ($\hat{\square} = \square|_{\lambda=\mathrm{i}j/2}$). According to this notation, taking the partial derivatives of expressions (2.74), (2.89), and (2.90) yields

$$c_k' = 2(\lambda + \mathrm{i}k)\lambda' - \mathrm{e}^{-(\lambda+\mathrm{i}k)2\pi} + b_0 2\pi\lambda'\mathrm{e}^{-(\lambda+\mathrm{i}k)2\pi}\,, \tag{2.92}$$

$$\hat{c}_k' = \left(2\pi b_0 (-1)^j + \mathrm{i}\,(j+2k)\right)\lambda' - (-1)^j\,, \tag{2.93}$$

$$\hat{D}_{-N}' = \left(2\pi b_0 (-1)^j \Gamma_{-N} + \mathrm{i}\Omega_{-N}\right)\lambda' - (-1)^j \Gamma_{-N}\,, \tag{2.94}$$

$$\hat{D}_{-N+1}' = \left(2\pi b_0 (-1)^j \Gamma_{-N+1} + \mathrm{i}\Omega_{-N+1}\right)\lambda' - (-1)^j \Gamma_{-N+1}\,, \tag{2.95}$$

where the coefficients

$$\begin{aligned}
\Gamma_{-N} &= 1\,,\\
\Omega_{-N} &= j - 2N\,,\\
\Gamma_{-N+1} &= \hat{c}_{-N} + \hat{c}_{-N+1}\,,\\
\Omega_{-N+1} &= \hat{c}_{-N}(j-2N+2) + \hat{c}_{-N+1}(j-2N)\,,
\end{aligned}$$

are real numbers, since $\hat{c}_k$ is real for all $k = -N, \ldots, N$. The same differentiation of equation (2.91) yields the recurrence

$$\hat{D}_k' = \hat{c}_k'\hat{D}_{k-1} + \hat{c}_k\hat{D}_{k-1}' - \frac{\varepsilon^2}{4}\hat{D}_{k-2}'\,, \quad k = -N+2, \ldots, N\,. \tag{2.96}$$

It can be proved by induction that (2.96) can be expressed in the same form as (2.94) and (2.95). If, for some k,

$$\hat{D}_{k-2}' = \left(2\pi b_0 (-1)^j \Gamma_{k-2} + \mathrm{i}\Omega_{k-2}\right)\lambda' - (-1)^j \Gamma_{k-2}\,, \tag{2.97}$$

$$\hat{D}_{k-1}' = \left(2\pi b_0 (-1)^j \Gamma_{k-1} + \mathrm{i}\Omega_{k-1}\right)\lambda' - (-1)^j \Gamma_{k-1}\,, \tag{2.98}$$

where Γ_{k-2}, Γ_{k-1}, Ω_{k-2}, Ω_{k-1} are real numbers, then, using (2.93), (2.96), we have

$$\hat{D}'_k = \left(2\pi b_0 (-1)^j \Gamma_k + \mathrm{i}\Omega_k\right)\lambda' - (-1)^j \Gamma_k\,, \quad k = -N+2, \ldots, N\,, \tag{2.99}$$

where the coefficients

$$\Gamma_k = \hat{D}_{k-1} + \Gamma_{k-1}\hat{c}_k - \frac{\varepsilon^2}{4}\Gamma_{k-2}\,,$$

$$\Omega_k = (j+2k)\hat{D}_{k-1} + \Omega_{k-1}\hat{c}_k - \frac{\varepsilon^2}{4}\Omega_{k-2}\,,$$

are again real numbers. Together with equations (2.94) and (2.95), this completes the induction.

The final round of recurrence is given by the case $k = N$. Equation $\hat{D}'_N = 0$ with $\hat{D}'_N$ defined in (2.99) gives

$$\mathrm{Re}\,\lambda' = \frac{2\pi\Gamma_N^2}{\left(2\pi b_0 (-1)^j \Gamma_N\right)^2 + \Omega_N^2} b_0\,. \tag{2.100}$$

The exponent-crossing direction along the D-curves is equal to the sign of $\mathrm{Re}\,\lambda'$. Since the coefficient of b_0 in (2.100) is positive, $\mathrm{sgn}(\mathrm{Re}\,\lambda') = \mathrm{sgn}(b_0)$. This means that moving away from the $b_0 = 0$ axis, each D-curve represents characteristic exponents becoming unstable, i.e., crossing the imaginary axis of the complex plane from left to right. The D-curves (2.86) and (2.88) are associated with single critical characteristic multipliers (i.e., $\mu = 1$ and $\mu = -1$, respectively), consequently, the number of unstable characteristic multipliers increases by one at each D-curve as $|b_0|$ is increased. So the only domains of stability are the triangles born from the stable triangles of the $\varepsilon = 0$ case. Since the case $\varepsilon = 0$ is already known (see Figure 2.4), the number of unstable characteristic multipliers can be determined for all the domains by equation (2.100) and by topological considerations. The stability chart can be seen in Figure 2.10 for $\varepsilon = 1$. The stable domains are indicated by gray shading. The frame view of the three-dimensional stability chart in the space $(\delta, b_0, \varepsilon)$ is shown in Figure 2.11.

2.4.4 Damped Case

The stability boundaries for the general damped and delayed Mathieu equation (2.63) with $\tau = 2\pi$ is more complex and they cannot be given in closed form. However, it can be shown that the stability boundaries associated with cyclic-fold and period-doubling (flip) bifurcations remains straight lines of slopes ± 1 in the plane (δ, b_0).

The analysis is very similar to that of the undamped case. Substitution of the trial solution (2.70), Fourier expansion of the periodic terms, application of trigonometric transformations, and balancing the harmonics results in the truncated determinant

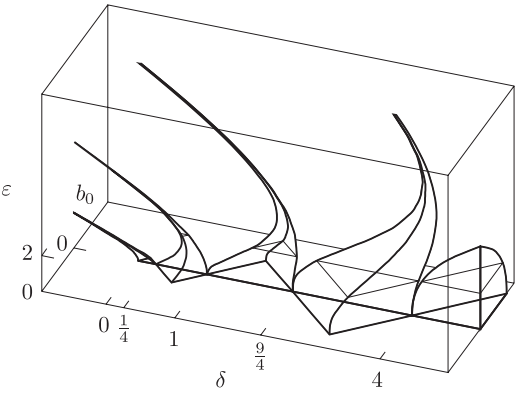

Fig. 2.11 Three-dimensional stability chart of the delayed Mathieu equation (2.69).

$$\tilde{D}(\lambda) = \det \begin{pmatrix} \tilde{c}_{-N} & \varepsilon/2 & & & \\ \varepsilon/2 & \tilde{c}_{-N+1} & \varepsilon/2 & & \\ & \ddots & \ddots & \ddots & \\ & & \varepsilon/2 & \tilde{c}_{N-1} & \varepsilon/2 \\ & & & \varepsilon/2 & \tilde{c}_N \end{pmatrix}, \tag{2.101}$$

where the diagonal elements have the form

$$\tilde{c}_k = \delta + (\lambda + \mathrm{i}k)^2 + a_1(\lambda + \mathrm{i}k) - b_0 \mathrm{e}^{-2\pi(\lambda+\mathrm{i}k)} \tag{2.102}$$

instead of c_k defined in equation (2.74).

After the substitution of $\lambda = \pm \mathrm{i}\omega$, $\omega \geq 0$, into (2.102), the imaginary part of $\tilde{c}_k$ reads

$$\operatorname{Im} \tilde{c}_k = a_1(\omega + k) + b_0 \sin(2\pi\omega) \,. \tag{2.103}$$

From this point, the proof of the undamped delayed Mathieu equation cannot be continued, since $\operatorname{Im} \tilde{c}_k = 0$ does not hold in the cases $\omega = j/2$, $j = 0, 1, \ldots$. This means that D-curves and stability boundaries may exist even for the case $\omega \neq j/2$, $j = 0, 1, \ldots$, and the critical characteristic multipliers can also be complex conjugate pairs of modulus 1. Consequently, secondary Hopf bifurcations may occur in this case, but the corresponding stability boundaries cannot be given in a simple closed form. However, the case $\omega = j/2$, $j = 0, 1, \ldots$, gives

$$\tilde{c}_k = \delta - (k + j/2)^2 - b_0(-1)^j + \mathrm{i}(k + j/2)a_1 \,, \tag{2.104}$$

and the same classification can be done as for the undamped case.

If j is even, that is, $j = 2h$, $h = 0, 1, \ldots$, then $\lambda = \mathrm{i}h$, and the corresponding characteristic multiplier is

$$\mu = \mathrm{e}^{\mathrm{i}h2\pi} = \mathrm{e}^{\mathrm{i}2\pi} = 1 \,. \tag{2.105}$$

In this case, $\tilde{c}_k = \delta - b_0 - (k+h)^2 + \mathrm{i}(k+h)a_1$, and $\tilde{D}(\lambda) = 0$ gives the relation $\tilde{f}_{+1}(\delta - b_0, \varepsilon, a_1) = 0$ for the D-curves. For the case $b_0 = 0$, the relation $\tilde{f}_{+1}(\delta, \varepsilon, a_1) = 0$ serves as the U_{+1} D-curves of the classical damped Mathieu equation defined in the form $\delta = \tilde{g}_{+1}(\varepsilon, a_1)$. This means that the linear D-curves exist for the $b_0 \neq 0$ case, too, in the form $\delta - b_0 = \tilde{g}_{+1}(\varepsilon, a_1)$. In the plane (δ, b_0), these are lines of slope +1 (shown as continuous lines in Figure 2.12). Along these D-curves, there exists a characteristic multiplier $\mu = +1$ representing a cyclic-fold bifurcation, and equation (2.63) has a periodic solution of period 2π.

If j is odd, that is, $j = 2h+1$, $h = 0, 1, \ldots$, then $\lambda = \mathrm{i}(h + 1/2)$, and the corresponding characteristic multiplier is

$$\mu = \mathrm{e}^{\mathrm{i}(h+1/2)2\pi} = \mathrm{e}^{\mathrm{i}\pi} = -1 \,. \tag{2.106}$$

In this case, $\tilde{c}_k = \delta + b_0 - (k+h+1/2)^2 + \mathrm{i}(k+h+1/2)a_1$, and $\tilde{D}(\lambda) = 0$ implies the relation $\tilde{f}_{-1}(\delta + b_0, \varepsilon, a_1) = 0$ for the D-curves. For the same reason as above, the D-curves exist again in the form $\delta + b_0 = \tilde{g}_{-1}(\varepsilon, a_1)$, where $\delta = \tilde{g}_{-1}(\varepsilon, a_1)$ gives the U_{-1} D-curves of the classical damped Mathieu equation. The D-curves are lines

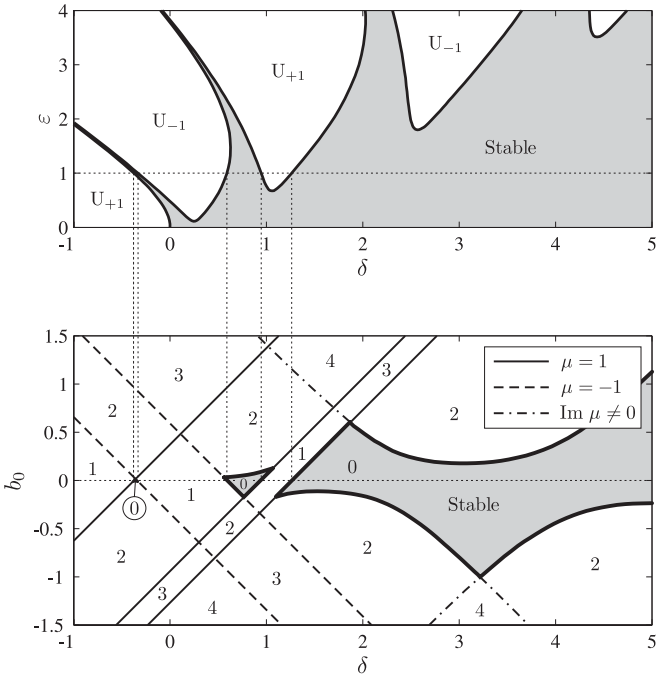

Fig. 2.12 Stability chart with the number of unstable characteristic multipliers for the damped delayed Mathieu equation (2.63) with $\tau = 2\pi$, $a_1 = 0.1$, $\varepsilon = 1$.

of slope -1 in the parameter plane $(\delta,\ b_0)$ (shown as dashed lines in Figure 2.12). Along these D-curves, there exists a characteristic multiplier $\mu = -1$ representing a period-doubling bifurcation, and equation (2.63) has a nontrivial periodic solution of period 4π.

This investigation showed that all the cyclic-fold and period-doubling D-curves are straight lines of slope ± 1 in the plane (δ, b_0). However, in addition to these linear D-curves, other D-curves associated with secondary Hopf bifurcation may also exist, since λ and consequently μ can also be complex at the loss of stability. These D-curves cannot be constructed based on the analysis of the corresponding Hill's deteminant (2.101) in closed form, but they can be determined by numerical techniques. Figure 2.12 presents the stability chart with the number of unstable characteristic multipliers determined by the semi-discretization method. The stable domains are indicated by gray shading. It can be seen that the straight lines obtained by the corresponding $\varepsilon = 1$ section of the Ince–Strutt diagram are indeed stability boundaries. These transition lines are shown as continuous and dashed lines for the $\mu = 1$ and $\mu = -1$ cases, respectively. The D-curves associated with complex characteristic multipliers are shown as dash-dotted lines.

http://www.springer.com/978-1-4614-0334-0

Semi-Discretization for Time-Delay Systems
Stability and Engineering Applications
Insperger, T.; Stepan, G.
2011, X, 174 p., Hardcover
ISBN: 978-1-4614-0334-0